Identification and Characterization of Interacting Proteins of TARANI/ Ubiquitin Specific Protease-14 in *Arabidopsis thaliana*

Anjana S. Hegde and Utpal Nath*

Department of Microbiology and Cell Biology, Indian Institute of Science, Bengaluru 560 012, India

*To whom correspondence should be addressed. Email: utpalnath@iisc.ac.in

Running title: Identification of TNI-interacting proteins

Keywords: TARANI, Ubiquitin protease 14, interacting proteins, Arabidopsis

Summary statement: The proteins that interact with the TARANI/ Ubiquitin protease 14 in vivo have been identified using immunoprecipitation mass-spectrometry methods. Identification of non-overlapping targets highlight the importance of using diverse protein identification methods.

Abstract

Ubiquitin proteases play a crucial role in protein degradation and turnover by regulating the cleavage of polyubiquitin chains. TARANI/UBIQUITIN SPECIFIC PROTEASE-14 (TNI/UBP14) specifically cleaves Lys-48-linked and linear polyubiquitin chains into mono-ubiquitins. The *tni* mutant exhibits pleiotropic phenotypes, including cup-shaped leaves, tri-cotyledons, reduced lateral roots, and increased petal number, though the underlying mechanisms driving these phenotypes remain unclear. In this study, we generated TNI transgenic lines and employed immunoprecipitation mass spectrometry, proximity labelling, and yeast two-hybrid screening to identify TNI's interacting proteins. These analyses revealed 92 interactors involved in diverse biological processes, including protein and carbohydrate metabolism, light signalling, and intracellular transport. Subcellular localization analysis showed that many of the interacting proteins are located in the nucleus and cytoplasm, suggesting that TNI's nuclear localization may regulate gene function. We further validated the

in planta biological significance of ULTRAPETALA 2 and HASPIN KINASE as key interacting partners of TNI. These findings uncover previously uncharacterized functions of TNI/UBP14, shedding light on its central role in cellular processes and providing insights into its regulatory mechanisms—an area that has remained largely unexplored until now.

Introduction

Proteins, essential for cellular processes function as part of complexes with other proteins. The specialized 26S proteasomal machinery ensures cellular protein homeostasis through continuous protein turnover, involving both ubiquitylation and deubiquitylation processes. Ubiquitylation, a crucial protein modification, governs various cellular processes. The coordinated action of E1 activating enzyme, E2 conjugating enzyme, and E3 ubiquitin ligase tags target proteins for degradation by adding ubiquitin. De-ubiquitylation reverses the E3 ligase function by hydrolyzing ubiquitin bonds (Clague et al., 2019). Ubiquitin proteasomal components play a fascinating dual role. Apart from their primary function in protein degradation, they also engage in non-proteasomal cellular activities. These include transcriptional regulation, epigenetic control, flowering, immune response, tissue growth, stress adaptation, and nutrient homeostasis within the cell. (Ferdous et al., 2002; Ezhkova et al., 2004; Cui et al., 2013; An et al., 2018; Cho et al., 2006; Ewan et al., 2011).

The ribosomal protein-anchored single ubiquitin or poly pro-ubiquitin chain is the de novo synthesis mode of ubiquitin. Iso-linked poly-ubiquitins are produced by cleaving the poly-ubiquitin chains from the target proteins during proteasome-mediated degradation. DUBs hydrolyse poly-ubiquitins from these sources to replenish the mono-ubiquitin pool. Arabidopsis genome encodes 64 DUBs, of which 27 are ubiquitin-specific proteases (UBPs) (Zhou et al., 2017).

The majority of the 26S proteasomal mutants show pleiotropic effects in plants. An amino acid substitution in the RPT5a subunit of the 26S proteasome led to Abscisic acid and ethylene-sensitive, and light hyposensitive mutants (Hayashi & Hirayama, 2016). The *rpn1a* mutation resulted in embryonic lethality in homozygous lines displaying arrest at the globular stage with defects in the embryonic root, protoderm, and procambium (Brukhin et al., 2005). UBIQUITIN SPECIFIC PROTEASE12/13 (UBP12/13 acts to) deubiquitinate the polyubiquitinated MYC2, opposing the activity of PLANT U-BOX 10 (PUB 10) E3 ligase, thereby stabilizing MYC2 and acting as a positive regulator of jasmonic acid response (Jeong et al., 2017). UBPs are also

involved in regulating flowering time and circadian clock. In the *ubp12ubp13* mutant, CONSTANS (CO) expression increased ahead of wild type in both short- and long-day conditions, followed by a subsequent rise in FLOWERING LOCUS T (FT) level resulting in early flowering phenotype. The observation indicates the significance of de-ubiquitination in flowering (Cui et al., 2013).

A forward genetic screen aimed at identifying the genetic mutants in Arabidopsis with altered leaf morphology identified the *tarani* (*tni*) ["boat" in Sanskrit] mutant, which exhibits a cup-shaped leaf phenotype as opposed to the flat leaf of wild-type (Karidas et al., 2015). *TNI* codes for ubiquitin-specific protease 14 (UBP14) which cleaves α-linked and isopeptide-linked poly-ubiquitin chains into mono-ubiquitin (Majumdar and Karidas et al., 2020). Arabidopsis contains a single copy of UBP14, and the null alleles of *UBP14* are embryonic lethal (Tzafrir et al., 2002), suggesting its evolutionarily conserved role(Majumdar & Nath, 2020).

AtUBP14 has an N-terminal ZnF-UBP domain followed by a protease domain and two consensus C-terminal UBA domains. The ZnF-UBP and UBA domains serve as interfaces in protein-protein interaction. UBP14 has been shown to localize in the nucleus to regulate endoreduplication in complex with the nuclear-localized proteins (Xu et al., 2016). UBP14 interacts with ULTRAVIOLET INSENSITIVE-4 (UVI4) (a cell cycle regulator in Arabidopsis) (Xu et al., 2016) and with multiple proteins in *Magnaporthe oryzae* (Wang et al., 2018). In the *tni* mutant, auxin repressors are found to be stabilized, leading to reduced auxin response, which is otherwise quickly degraded by the 26S proteasome pathway upon auxin signalling (Majumdar & Karidas et al., 2020). The ZnF-UBP domain in TNI led us to hypothesize that this essential protease, central to the ubiquitin-proteasome system (UPS), interacts with multiple proteins to regulate various cellular processes, resulting in its pleiotropic phenotypes. Recognizing that proteins often function within complexes, we set out to uncover the unknown functions of TNI by identifying its interacting partners

Protein–protein interactions (PPI) are fundamental for understanding cellular nature. Over the past two decades, proteomic studies have evolved from whole-cell analyses to organelle-specific, tissue-specific, and stage-specific identifications. These advancements empower scientists to unravel cell functions through increased proteomic knowledge. Numerous research groups have reported organelle-specific and tissue-specific proteomes.

The advancement in protein tagging techniques enabled the identification of the organelle and tissue-specific low-expressed proteins. The stochastic interaction is challenging to study in the

biological system. A modified version of the biotin ligase BioID from *E.coli* was developed to map protein interactions (Roux et al., 2012). The feasibility and non-lethal nature of biotin led to its popularity quickly, and now it is one of the preferred techniques for protein identification. It has been employed in other biological systems like mammalian and plant cells (Kim et al., 2016). TurboID, the modified version of BioID, is efficient in labelling yeast, flies, worms, chickens, mammals, and plant cells within 10 minutes (Branon et al., 2018). The task of identifying nuclear membrane interactors was made easy by BioID tagging (Huang et al., 2020). Proximity labelling made these types of studies possible with minimal tissue and without much loss of the sample (Roux et al., 2012, Kim et al., 2016, Branon et al., 2018). Protein-protein interaction studies are crucial to understanding cellular functions. Since cellular processes are dynamic, more than one method of interaction is preferred. The constant turnover or the movement of the proteins in the cell results in variation in the immediate environment. Hence, we decided to broaden our approach to identify TNI interactors by distinct methods.

We identified the *in planta* interactors of TNI by immunoprecipitation-mass spectrometry (MS), proximity labelling and transcription factors by yeast two-hybrid screening. We validated a few select interactors from the high throughput screen using binary methods. ULTRAPETALA 2, a trithorax family protein involved in regulating petal number, interacts with TNI. We showed that the haspin kinase protein is stabilized in the *tni* mutant.

Results

Generation of TNI transgenic lines

We generated transgenic Arabidopsis lines expressing *TNI* under *35S* CaMV promoter, *RPS5A* promoter, and endogenous *TNI* promoter in the Col-0 background. A detailed phenotypic analysis of these transgenic lines in the T2 generation revealed that nearly 20% of the transgenic plants show cup-shaped leaves similar to the *tni* mutant (Fig. 1A). Further, expression of the transgenic TNI protein was confirmed using western blot analysis (Supp Fig. 1A). TNI protein expression was also visualized in different tissues of *pTNI::TNI-GUS* transgenic line. GUS assay showed that TNI is expressed almost throughout the plant and at all stages of plant growth, as was reported earlier (Doelling et al., 2001). TNI-GUS signal was detected throughout the plant in the seedling stage (Fig. 1B) and in carpel, filament, stalk, petals, and sepals. Since protein expression was observed throughout the seedling, we chose 8-day-old seedlings for the *in vivo* protein interaction experiments. TNI was previously shown to

be localised to the nucleus in the *Nicotiana* leaves when over-expressed under *35S* promoter (Xu et al., 2016). We generated a transgenic line expressing the TNI-G3GFP protein to check the subcellular localisation of TNI in the cell. TNI was found to be localised to both nucleus and cytoplasm (Fig. 1C). Previously, it was reported that the lateral root number is significantly less and hypocotyl is two times longer in the *tni* mutant than in the Col-0 (Majumdar and Karidas et al., 2020). Lateral root number was significantly more and hypocotyl length was significantly longer in the TNI overexpression transgenic lines (Fig. 1D, E). The belowground phenotypes of TNI transgenic lines contrast with that of the *tni* mutant.

Identification of interacting proteins of TNI

a. By Immunoprecipitation-MS (IP-MS)

We selected the *RPS5a::TNI-Myc* transgenic line to perform an immunoprecipitation-pulldown experiment. The total protein extract from the *RPS5a::TNI-Myc* seedlings was pulled down against anti-Myc and anti-IgG antibodies (Fig.2A). We conducted experiment with three biological replicates, including respective controls, and confirmed the equal amount of TNI in all the replicates (Supp Fig. 1B). The presence of TNI was validated by anti-Myc immunoblot in both the anti-Myc and anti-IgG pulldown (~120kDa) (Fig. 2B). We found 29 proteins enriched in the anti-Myc pull-down against the IgG negative control (Fig. 2C and Table 1).

The proteins identified at least two times in a group were chosen, and an enrichment graph was plotted for sample and control with changes in various parameters. In the final list of 29 proteins, 28 were selected showing enrichment with FDR=0.05, S=2.0, and one with FDR=0.01, S=0.1. TNI profile plot showed an increase in LFQ intensity values in the samples compared to the controls. The identified 29 proteins showed a similar pattern to TNI in their respective LFQ intensity profile plot (Supp Fig. 2A).

b. By Proximity labelling affinity Purification-MS (AP-MS)

The wild type, *pTNI::TbID-Myc,* and *pTNI::TbID-TNI-Myc* seedlings were treated with the biotin. TbID is a biotin ligase enzyme that covalently adds biotin to the proteins within the radius of 10 nm (Roux et al., 2012). Seedlings without biotin treatment were taken as a negative control (Fig. 2D). We confirmed the expression of TbID-TNI(~150kDa) and TbID (~60kDa) with 50 µM biotin treatment (Supp Fig. 1C&D) using anti-Myc antibody. After confirming the transgenic protein expression, we standardised the biotin treatment. Based on the previous literature study (Mair et al., 2019), we selected concentrations ranging from 0-200 µM. We saw a slight increase in the total biotinylated protein from 20 µM to 50 µM biotin concentration

and from 30 minutes to 1 hour; it remained stable afterwards. For better enrichment in the mass spectrometry, we treated seedlings for 3 hours. Seedlings 5, 6, 8, and 10 days old were treated and checked for any stage-specific increase in biotinylation (Supp Fig 3A to F). We found no difference in biotinylation with the age of seedlings. Hence, we selected eight-day-old seedlings and treatment for 3 hours with 50 µM biotin concentration for further experiments. We confirmed the pulldown of biotinylated proteins by SA-HRP blotting (Fig 2E).

We found 19 interacting proteins from the final list of treated to untreated controls (Fig 2F and Table 1). The enriched proteins in each combination between six samples above FDR=0.05 and S=2.0 were selected, and the proteins enriched only in the sample set were considered interactors. LFQ intensity and heat map of identified proteins across the samples and controls are plotted (Supp Fig 4&5). Further, we categorized TNI interactors from IP-MS and AP-MS according to their subcellular localization. We found that the highest number of interactors are nuclear-localized proteins, followed by cytoplasm, plastid, Golgi, and extracellular proteins, respectively (Fig 2G).

c. Yeast Two-Hybrid Assay

TNI localizes to the nucleus (Xu et al., 2016). We were interested to see the TNI interaction with the transcription factors. Initially, we checked the suitable condition for the yeast two-hybrid screening. *pDEST32-TNI* and its truncated versions *pDEST32-ΔZnF, pDEST32-ZnF, pDEST32-ΔUBA*, and *pDEST32-UBA* were used for autoactivation screening (Fig. 3 A). TNI, ΔZnF, *ZnF,* and ΔUBA showed autoactivation in the $Leu^{-}His^{-}$ and $Leu^{-}His^{-}$+10-30 mM 3-aminotriazole (3-AT). However, growth was not observed on $Leu^{-}Ade^{-}$ and $Leu^{-}His^{-}Ade^{-}$ plates (Fig. 3 B). UBA domain alone showed growth in the presence of $Leu^{-}His^{-}$+10-30 mM 3-AT, $Leu^{-}Ade^{-}$, and $Leu^{-}His^{-}Ade^{-}$. Hence, we chose to perform a yeast-two hybrid assay with full-length TNI and screened for positive interactors on $Leu^{-}Ade^{-}$ and $Leu^{-}His^{-}Ade^{-}$ plates as autoactivation was not observed under these selection conditions.

TNI interacts with the transcription factors.

We selected 197 transcription factors from the Arabidopsis prey protein library to perform a yeast two-hybrid screen using TNI as bait. Our criteria for selection were: (i) transcription factors regulating plant signalling pathways well known to be degraded by the 26S proteasomal system (Ramos et al., 2022, Carlos et al., 2000,Hellmann & Estelle, 2002,Li et

al., 2017); (ii) Arabidopsis homologs of the *M.oryazae* transcription factors which interacted with the UBP14 of the *M.oryazae* (Wang et al., 2018); and (iii) predicted TNI-interactors from the STRING database (https://string-db.org) A total of 44 transcription factors interacted with TNI on the *Trp⁻Leu⁻Ade⁻* and *Trp⁻Leu⁻His⁻Ade⁻* selection plates (Fig. 3C and Table 1).

We grouped the interactors according to the transcription factor family they belong to. In Arabidopsis, AP2-EREBP, WRKY, and NAC members are the highest on the list, which are present only in the plants(Riechmann et al., 2000). We saw maximum interactors from the AP2-EREBP, WRKY, and NAC families (Fig. 3D).

GO analysis

The interacting proteins are reportedly involved in biological processes like hormone signalling, response to environmental stimuli, signal transduction, secondary cell wall biogenesis and molecular functions like carbohydrate metabolism, nucleotide binding, and hydrolase activity (Fig. 4 A&B). From the STRING database, we found that some groups of proteins have previously been reported to interact. ULTRAPETALA2 (ULT2), ULTRAPETALA1 INTERACTING FACTOR1 (UIF1), and TUBBY-LIKE PROTEIN 2 (TLP2) are found by text-mining. Co-expression of LATE ELONGATED HYPOCOTYL (LHY) and PSEUDO RESPONSE REGULATOR (PRR9) is reported from the curated databases. DEAD BOX RNA HELICASE 1 (DRH1) interacts with ERBB-3 BINDING PROTEIN 1 (EBP1), and EBP1 forms a ternary complex with ELONGATION FACTOR (EF1A) and ELONGATION INITIATION FACTOR 3 (EIF3) (Fig 4C).

HASPIN kinase is stabilized in the *tni* mutant

We found enrichment of haspin kinase in the IP-MS suggesting it could be strong interactor of TNI (Supp Fig 2) Haspin kinase is involved in phosphorylating Thr3 and Thr11 at histone 3 as shown *in vitro* (Ashtiyani et al., 2011; Kurihara et al., 2011) and *in vivo* (Kurihara et al., 2011). We found haspin kinase as one of the interactors with the highest LFQ intensity, as shown in the intensity profile plot in the IP-MS approach (Supp Fig 2A). The downregulation of haspin exhibited multiple shoots, abnormal flowers, semi-fertile and undeveloped siliques. The overexpression lines showed multi-rosette and adventitious shoot apical meristems (Ashtiyani et al., 2011). The *tni* mutant shows increased petal number, decreased shoots, undeveloped siliques, and reduced seed number(Karidas et al., 2015; Majumdar and Karidas et al., 2020). Hence, we were interested in checking the level of haspin protein in the *tni* mutant. The Haspin-

GFP protein level was found to be increased in the *Haspin-GFP #1*tni* line than in the *Haspin-GFP #1* (Fig 5A&B). Haspin-GFP band was detected in the *Haspin-GFP #1*tni* but not in the *Haspin-GFP #1* as confirmed by western blotting using anti-GFP antibody (Fig 5C). The seed number was found to be reduced in *HASRNAi #23.2* and *HASRNAi #14.1* but not in *HASRNAi #25.1* compared to Col-0. Seed number was significantly reduced in the *HASRNAi #14.1*tni* but not in the *HASRNAi #23.2*tni,* and *HASRNAi #25.1*tni* compared to *tni* alone (Fig 5D). The seed number was reduced in overexpression lines of haspin namely *35S::HASPIN #2.1, 35S::HASPIN #10.2* than in Col-0 but *35S::HASPIN #2.1*tni, 35S::HASPIN #10.2*tni* did not show a difference compared to *tni* mutant (Fig 5E). This suggests that TNI is destabilizing the haspin kinase even upon overexpression of haspin resulting in reduced seed number compared to the wild type. The seed number is less in overexpression of haspin in the *tni* mutant background. The reason might be some amount of TNI is still functional in the *tni* mutant which is degrading haspin or the involvement of other pathways. Reduced seed number in haspin downregulation in either wild type or *tni* mutant background suggests that TNI could be acting upstream to haspin kinase.

ULT2 interacts with TNI

We validated the interaction of the ULT2 from the Y2H screen and TNI by bimolecular fluorescence complementation (BiFC) assay. We observed that ULT2-nEYFP interacts with the TNI-cEYFP upon co-expression in the Nicotiana leaf (Fig 6). ULT2 is involved in regulating flower petal numbers along with another member of the family, ULT1. The *ult1-2 ult2-3* double mutant shows an increase in petal number similar to the *tni* mutant. Probably TNI interaction stabilises ULT2 to regulate the petal number. We have also found UIF1, another TF involved in regulating flower petal numbers. UIF1 interacts with ULT1 (Moreau et al., 2016) and ULT1 interacts with ULT2 (Monfared et al., 2013). It's also possible that ULT1, ULT2, and UIF1 might be interacting in a complex with TNI.

Discussion

We used three different approaches to identify a more complete TNI interactome that would generate a fair understanding of the role of TNI/UBP14 in plant development. TNI/UBP14 is present throughout all stages of growth and in all tissues. TNI/UBP14 is essential in maintaining plant protein homeostasis. The absence of TNI/UBP14 causes embryonic lethality, and its hypomorphic alleles are recessive (Karidas et al., 2015; Tzafrir et al., 2002; Xu et al.,

2016). This suggests the importance of the TNI/UBP14 in the UPS system. It has been shown that TNI/UBP14 can bind to the free polyubiquitin chain and disassemble it (Majumdar and Karidas et al., 2020). It is likely that TNI/ UBP14 also cleaves the ubiquitin moiety from target proteins as well. Our study was aimed to identify those target proteins by identifying TNI-interacting subset of the proteome.

From the three approaches used here, we found proteins involved in diverse biological processes including cell wall remodelling, stress response, carbohydrate metabolism, protein synthesis, chaperones, histone-associated proteins and epigenetic modifiers. Interestingly, nearly half of the interacting proteins are predicted to function as enzymes, suggesting the role of TNI/UBP14 in diverse biological processes in the cell. Among the interactors, several proteins exhibit functional similarity and are grouped under the same pathway.

An intriguing outcome of our study is the lack of overlapping interacting proteins among the subsets identified in various methods. The non-overlapping targets perhaps indicate that a more inclusive approach should be taken in future to identify the full repertoire of the interacting proteins of a specific bait. It has been demonstrated that sometimes the same method used for identifying interacting proteins identifies targets with minimal overlap. For example, a comparative bioinformatic analysis found merely ~20% overlapping proteins from the union of three large-scale Y2H screenings aimed to identify protein-protein interaction in yeast (Yu et al., 2008).

Since we were interested in building a comprehensive interactome of TNI/UBP14, employing approaches with different principles best suited our purpose. The yeast two-hybrid study, the IP-MS study, and the AP-MS protocol are fundamentally different in their approach and, hence, explains the outcome of non-overlapping target proteins from these experiments. Y2H study is a out-of-context, condition-specific investigation focussing on interaction upon nuclear localization and tends to show results with transient interactors. *In vivo* approaches such as IP-MS detect stable interactors, whereas AP-MS identifies proteins that make stable complex with the bait as well as those that come in proximity to the bait without even making any direct contact (Roux et al., 2012).

As TNI/UBP14 is a ubiquitin protease, we examined whether any interacting target proteins identified are known to be ubiquitinated and targeted for degradation by the UPS. We compared the TNI/UBP14 interacting with reported ubiquitinated protein database. We identified thirty-two proteins from our dataset that are reported to be present in the Arabidopsis proteome

subsets where a pull-down experiment was performed to identify ubiquitinated proteins (Kim et al., 2013; Song et al. 2021) (Fig. Supp 6 A, B). This suggests that the TNI-interacting proteins perhaps are degraded by 26S proteasomal machinery. However, the ubiquitination status of the target proteins identified in our study should be compared between wildtype and *tni* mutant plants, and this remains a major limitation of our work.

When we compared our interacting proteins with the STRING database (https://string-db.org/) proteins from either a single method or all three methods used in our study formed complexes to perform specific functions. The largest complex we identified was of eleven protein nodes with ten edges involved in protein synthesis. We also found that several target proteins are co-expressed with TNI, including BETA-GALACTOSIDASE 1, BETA-XYLOSIDASE 1, BETA-GALACTOSIDASE 4 involved in cell wall remodelling, ULT2, UIF1, and TLP 2 involved in regulating flower petal number, REGULATOR OF AXILLARY MERISTEM 2 (RAX2), and NO APICAL MERISTEM 031 (NAC031) involved in axillary branching. Physical interaction of FILAMENT TEMPERATURE-SENSITIVE MUTANT 2 (FTSZ2), CALMODULIN 12 (CML12) and, FRUCTOSE BISPHOSPHATE ALDOLASE 3 (FBA3), FBA6, and GLYCERALDEHYDE 3 PHOSPHATE DEHYDROGENASE A SUBUNIT 2 (GAPA2), which appeared in STRING analysis, is well reported (Fig. 3C).

We have validated the interaction of the selected interactors by other binary methods. Haspin stabilization in the *tni* mutant suggests that TNI/UBP14 is required for the degradation of haspin in the wild type. Considering the broad range interactome of TNI/UBP14 and the pleiotropic phenotype of its mutant (Karidas et al., 2015; Xu et al., 2016), it would be interesting to examine the biological significance of TNI interaction with these diverse interactors. An in-depth study on the affinity of TNI towards ubiquitinated or non-ubiquitinated states is necessary to understand the biological function of these interactions in plants.

Materials and Methods

Plant materials and growth conditions

Seeds were surface sterilized and stratified in darkness for three days at 4°C; they were transferred to the growth chamber and kept in light for 6-9 hours. Later, plates were kept under dark conditions for three days to select the transformants in hygromycin selection and shifted

back to light. Plants were maintained under long-day conditions with 16 h light (120 μmol/m^2/s) and 8 h dark, 22°C. All transgenic lines were generated in the Col-0 background. To perform the TNI protein pulldown experiments, seedlings were sown on half MS medium and stratified in the dark at 4°C for two to three days. Later, plates were shifted to light and maintained under the long-day condition with 16 h light (120 μmol/m^2/s) and 8 h dark, 22°C.

Construct generation and plant transformation

The TNI CDS (2394 bp) was subcloned by amplifying from the *TNI-pGEX4T1* using CDS-specific primers with 5' attB1 and 3'attB2 sites and cloned into the entry vector pDONOR221 by BP Clonase reaction (Invitrogen). TNI promoter was amplified from the *pTNI-pCAMBIA* (Premananda Karidas, PhD thesis, 2014) using promoter-specific primers with 5' attB4 and 3'attB1R sites, respectively, and cloned by pENTR™ 5'-TOPO™ TA Cloning™ kit (Invitrogen). Turbo ID was amplified from the vector *pVHS64* (Prof. P.V. Shivaprasad acknowledged), and it is cloned to the N-terminus end of the TNI in the vector *TNI-pGEX4T1* by Gibson Assembly Master Mix (E2611S, NEB). *TbID -TNI* was amplified by CDS-specific primers with 5'attB1 & 3'attB2 sites and cloned into the pDNR221 vector by the BP clonase reaction (Invitrogen). 35S promoter was amplified from the pCAMBIA1301, and the RPS5A promoter was amplified from the plasmid pRPS5A_ER8_GW (Prof. Ram Yadav & Prof. Nam Hai Chua acknowledged) using promoter-specific primers with 5' attB4 and 3'attB1R site respectively and cloned into the entry vector pDONOR P4-P1R by BP Clonase reaction (Invitrogen). Further, promoter and CDS entry clones are incorporated into the R4pGWB vectors (spectinomycin selection) with the C-terminal reporter tags R4pGWB 510-FLAG, R4pGWB 519-10xMyc, R4pGWB 533-GUS, R4pGWB 543-G3GFP by tripartite LR reaction (Invitrogen). All the clones were transformed into the *Agrobacterium tumifaciens* GV3101 strain by electroporation (Biorad, 2.5Hz, 5 seconds). Positive clones were selected, and floral dipping was performed in Col-0 plants. Transformants were selected on MS medium (Himedia) containing 100 μg ml^{-1} cefotaxime sodium salt (Himedia) and 20 μg ml^{-1} hygromycin (Sigma-Aldrich).

Construct generation and Yeast two-hybrid assay

TNI CDS from *pDONOR221-TNI* (see above) was moved C-terminal to the GAL4 DNA-binding domain (GAL4-DBD) in pDEST32 vector by LR reaction (Invitrogen). and introduced

into yeast strain AH109 by the LiOAc/ssDNA/PEG method (Gietz et al., 1992; Bartel et al., 1993; Harper et al., 1993). Transformants were selected on a synthetic drop-out medium lacking leucine. A prey library of 1956 Arabidopsis transcription factors C-terminal to the GAL4 DNA-activation domain (GAL4-AD) in the vector pDEST22 was received in the form of bacterial glycerol stocks from the ABRC stock center (Pruneda-Paz et al., 2014). Plasmid isolation was carried out from the complete library, and in those, 197 plasmids were transformed individually into the previously transformed AH109 yeast strain expressing TNI by the standard LiAc protocol and grown on *Leu⁻His⁻* +3AT, *Leu⁻Ade⁻, Leu⁻His⁻ Ade⁻* selection as described in the Yeast Protocols Handbook (Clontech, http:// www.clontech.com)

Immunoblot -analysis

Protein extraction was carried out from 29-30-day-old leaves using protein extraction buffer (50 mM Tris-HCl pH 7.4, 150 mM NaCl, 10mM MgCl2, 0.1% (v/v) NP-40,1 mM PMSF, and 1X complete protease inhibitor cocktail (Roche)). The crude extract was centrifuged at 12,000g for 15 min at 4°C. Protein concentration was measured by Bradford assay, and equal concentrations of protein were loaded into the 10% (v/v) SDS-PAGE, transferred to PVDF membrane (Millipore, USA), and immunoblotted using anti-MYC (#2276, CST), and anti-GFP(#3H9, Chromotek) primary antibodies and anti-Mouse (Sigma), and anti-rat secondary antibodies. ECl (Millipore, USA) was used to develop the blots. For the biotin-treated seedlings, the PVDF membrane was blocked in 5% BSA and incubated in streptavidin-HRP (S911, Thermo Fisher Scientific) for 1 hour, and proceeded to develop.

Bimolecular Fluorescence Complementation assay

pDONOR221-TNI and *pDONOR221-ULT2* was cloned into the *pSITE-cEYFP-N1* and *pSITE nEYFP*-C1 by LR reaction respectively. Further, these clones were transformed into the Agrobacterium tumifaciens GV3101 strain by electroporation, including the empty BiFC binary vectors. (Biorad, USA, 2.5Hz, 5 seconds). Positive clones were selected, and the primary culture was grown overnight in the presence of respective Antibiotic selection. Inoculum from the primary culture was used for the secondary culture for four hours of growth at 30°C. Cells were pelleted down at 4000rpm, 20 minutes at 4°C. The pellet was resuspended in the MES buffer (100 mM MES-KOH, pH 5.6, 10 mM MgCl2, 15 mM Acetosyringone) to

OD600=0.8. The respective cultures were mixed in equal volumes and incubated on ice for one hour. The cultures were infiltrated onto the abaxial side of the 3–4-week-old Nicotiana leaves and plants were watered well and kept in the dark for 24 hours. Then, the plants were shifted to light for 24-36 hours, and the leaves were DAPI stained and observed under the confocal microscope with EYFP (514nm) and DAPI (358nm) 405 diode, Argon multiline laser under 10X magnification (Zeiss 880 Multiphoton, Germany).

Immunoprecipitation-pulldown

The eight-day-old *RPS5a::TNI-Myc* seedlings grown in half MS medium were treated in 20 µM MG132 for 16hrs at 22°C. Seedlings were tap-dried, snap-frozen, and stored at -80°C. Seedlings were ground in IP buffer I (50mM HEPES pH 7.4, 50mM NaCl,10mM EDTA, 0.1% TritonX-100, 1mM PMSF, 0.1mg/ml Dextran, 1X complete protease inhibitor cocktail (Roche), 50 µM MG132) and centrifuged at 12,000rpm for 20 minutes at 4°C. The supernatant was separated, and protein concentration was measured by the Bradford method. Protein extract from *RPS5a::TNI-Myc* seedlings were incubated with anti-Myc magnetic beads (#5698S, CST) and anti-IgG mouse (#5873S, CST) at 4°C on a rotor for 5hrs. Beads were separated by a magnetic stand and washed twice in IP buffer II (50mM HEPES pH 7.4, 50mM NaCl, 10mM EDTA), once in IP buffer III (50mM HEPES pH 7.4, 150mM NaCl,10mM EDTA) and once in 1X PBS, pH 7.4. The buffer was removed entirely from the beads and stored at -80^{0}C until proceeded for the on-bead digestion.

Affinity Purification by streptavidin beads

Eight-day-old Col-0, *pTNI::TbID-Myc,* and *pTNI::TbID-TNI-Myc* seedlings grown on half MS were treated with 50 µM biotin for 3hrs at 22°C, and biotinylation was stopped by washing in ice-cold water three times for three minutes each. Seedlings were tap-dried and snap-frozen, and an aliquot was taken for immunoblot analysis. Protein was extracted in extraction buffer as mentioned in Mair et al., 2019 (50mM Tris pH 7.5, 150mM NaCl, 1mM EGTA, 1Mm DTT, 0.1% SDS, 1% TritonX-100, 0.5%Sodium deoxycholate, 1X complete protease inhibitor cocktail (Roche),1mM PMSF) and kept at 4°C for 15 minutes on rotor wheel. Protein extract was centrifuged at 12,000 rpm for 15 minutes at 4°C. The supernatant was separated and depleted of extra biotin by passing through the PD-10 desalting column (GE-Healthcare).

Protein concentration was measured by Bradford assay, and an equal concentration of protein was taken and incubated with Dynabeads MyOne Streptavidin C1 (#65002, Invitrogen) overnight at 4°C on the rotor. Beads were separated on a magnetic rack and washed in respective buffers, as described in Branon et al. (2018). Beads were washed with 1 ml each of the following solutions on rotor 2x with cold extraction buffer at 4°C, 1x with cold 1M KCl at 4°C, 1x with cold 100 mM Na_2CO_3 at 4°C, 1X with 2M Urea in 10mM Tris pH 8.0 at room temperature and 2X with cold extraction buffer without complete protease inhibitor and PMSF at 4°C. 20ul or 2% of the beads were boiled in 20 ml 4x Laemmli buffer with 20 mM DTT and 2 mM biotin at 98˚C for 15 min for immunoblots. Buffer was removed from the rest of the beads and stored at -80°C until further procedure.

MS Sample Preparation

On-bead trypsin digestion was performed to digest the proteins. Beads were washed twice in 50 mM Tris pH 7.5 and 1 ml of 2M urea in 50 mM Tris pH 7.5. Beads were incubated at 25°C for 3 hrs with shaking in 80ul of Trypsin buffer (50 mM Tris pH7.5, 1M Urea, 1 mM DTT, 0.4µg Trypsin). The supernatant was transferred to a new tube, and beads were washed twice in 60ul of 1M Urea in 50 mM Tris pH7.5. Eluates were pooled and reduced by adding DTT to a final concentration of 4 mM and incubated at 25°C for 30 minutes. Alkylation was performed by 10 mM Iodoacetamide to final concentration followed by 0.5µg Trypsin digestion overnight at 25°C with shaking. The next day, the supernatant was separated from the beads and desalted on Pierce ™ C18 Spin columns (# 89873, Thermo Scientific).

LC-MS/MS

In the LC-MS/MS run, peptides were resuspended in 0.1% formic acid and 0.1% acetonitrile. Samples were analyzed in a PepMap™ RSLC C18 Nano liquid chromatography-Orbitrap Fusion mass spectrometer (Thermo Fisher). Peptides were separated by PN ES803A rev.2 (Thermo Fisher) analytical column. The flow rate was 250 nl/min, and a 160 min gradient was used. Elution of the peptide was done in a 5% to 95% gradient of solvent B (80% acetonitrile, 0.1% formic acid, 20% water) with a corresponding gradient of solvent A (0.1% formic acid) for 160 minutes, followed by 60 min wash in solvent B. Precursor Scan Range(m/z) was 350 to 2000 and 20 topmost intense charged precursors were selected for fragmentation.

Fragmentation was done by Orbitrap-higher energy collision dissociation (OT/OT/HCD) with 30% HCD collision energy.

MS data analysis

Protein identification was performed in Max Quant (version 2.4.2.0) with minor modifications in the default settings. The parameters for the antibody-mediated pulldown experiment are as follows: Control IgG pulldown and sample anti-Myc pulldown were set as fractions 1 and 2, respectively. Under the "Group-specific parameters," oxidation (M) and acetyl (Protein N-term) were set as variable modifications with a maximum of five modifications per peptide. 'Digestion' was set to Trypsin/P, with two maximum missed cleavages. The minimum ration count was set to one with Normalization Type-Classic under the 'Label-Free Quantification.' In the "Global parameters," Oxidation(M) and Acetyl (Protein N-term) are set as modifications used in the protein quantification. "Unique+Razor peptides" were used for quantification. PSM FDR and Protein FDR were set to 0.01, and the Match between runs was selected under 'Identification.' Peptides were searched against the TAIR10 database (Araport_pep_20220103, updated on 2022-01-03, www.arabidopsis.org) with 48231 protein entries with additional MYC, trypsin and keratin as contaminants. The minimum peptide length was set to seven.

The settings were set as above, with slight changes for the enzyme-based proximity labeling approach. Fractions were set from 1-6 for the untreated and treated Col-0, Turbo, and Turbo-TNI, respectively. Carbamidomethyl(C) is under fixed modification, and Trypsin is under the 'Digestion.' Peptides were searched against the TAIR10 database (Araport_pep_20220103, updated on 2022-01-03, www.arabidopsis.org) with 48231 protein entries with additional MYC, and TurboID sequences as contaminants.

Confocal imaging

The root tip of the 8 DAS of *pTNI::TNI-G3GFP*, *HASPIN-GFP* and *HASPIN-GFP*tni* were imaged under the confocal microscope with the GFP (395nm), Argon multiline laser under 10X magnification (Zeiss 880 Multiphoton, Germany).

Statistical analysis

The 'proteinGroups.txt' file was uploaded to Perseus (version 2.0.7.0) for the statistical analysis. T-test, Histogram, Profile plot, Heat map, and PCA analysis were performed in Perseus. Subcellular localization prediction was done in SUBA5 (https://suba.live), and results were exported to R Studio (version 4.3.0) for plotting the graph. Gene Ontology analysis was performed in Shiny GO (V0.80)(Ge et al., 2020) and STRING database (version 12.0). Graphs were plotted in R Studio (version 4.3.0).

References

Ashtiyani, R. K., Moghaddam, A. M. B., Schubert, V., Rutten, T., Fuchs, J., Demidov, D., Blattner, F. R., & Houben, A. (2011). AtHaspin phosphorylates histone H3 at threonine 3 during mitosis and contributes to embryonic patterning in Arabidopsis. *Plant Journal*, *68*(3), 443–454. https://doi.org/10.1111/j.1365-313X.2011.04699.x

Branon, T. C., Bosch, J. A., Sanchez, A. D., Udeshi, N. D., Svinkina, T., Carr, S. A., Feldman, J. L., Perrimon, N., & Ting, A. Y. (2018). Efficient proximity labeling in living cells and organisms with TurboID. *Nature Biotechnology*. https://doi.org/10.1038/nbt.4201

Brukhin, V., Gheyselinck, J., Gagliardini, V., Genschik, P., & Grossniklaus, U. (2005). The RPN1 subunit of the 26S proteasome in Arabidopsis is essential for embryogenesis. *Plant Cell*. https://doi.org/10.1105/tpc.105.034975

Carlos Del Pozo, J., & Estelle, M. (2000). F-box proteins and protein degradation: An emerging theme in cellular regulation. *Plant Molecular Biology*, *44*, 123–128.

Cui, X., Lu, F., Li, Y., Xue, Y., Kang, Y., Zhang, S., Qiu, Q., Zheng, X. C., Cui, X., Zheng, S., Liu, B., Xu, X., & Cao, X. (2013). Ubiquitin-specific proteases UBP12 and UBP13 act in circadian clock and photoperiodic flowering regulation in Arabidopsis. *Plant Physiology*, *162*(2), 897–906. https://doi.org/10.1104/pp.112.213009

Doelling, J. H., Yan, N., Kurepa, J., Walker, J., & Vierstra, R. D. (2001). The ubiquitin-specific protease UBP14 is essential for early embryo development in Arabidopsis thaliana. *Plant Journal*, *27*(5), 393–405. https://doi.org/10.1046/j.1365-313X.2001.01106.x

Ge, S. X., Jung, D., Jung, D., & Yao, R. (2020). ShinyGO: A graphical gene-set enrichment tool for animals and plants. *Bioinformatics*, *36*(8). https://doi.org/10.1093/bioinformatics/btz931

Hayashi, S., & Hirayama, T. (2016). ahg12 is a dominant proteasome mutant that affects multiple regulatory systems for germination of Arabidopsis. *Scientific Reports*, *6*(May), 1–12. https://doi.org/10.1038/srep25351

Hellmann, H., & Estelle, M. (2002). Plant development: Regulation by protein degradation. *Science*, *297*(5582), 793–797. https://doi.org/10.1126/SCIENCE.1072831/ASSET/9454C099-9BA7-4DFB-9A8B-E107BC26FEE3/ASSETS/GRAPHIC/SE3020737002.JPEG

Huang, A., Tang, Y., Shi, X., Jia, M., Zhu, J., Yan, X., Chen, H., & Gu, Y. (2020). Proximity labeling proteomics reveals critical regulators for inner nuclear membrane protein degradation in plants. *Nature Communications*, *11*(1). https://doi.org/10.1038/s41467-020-16744-1

Jeong, J. S., Jung, C., Seo, J. S., Kim, J. K., & Chua, N. H. (2017). The deubiquitinating enzymes UBP12 and UBP13 positively regulate MYC2 levels in jasmonate responses. *Plant Cell*, *29*(6), 1406–1424. https://doi.org/10.1105/tpc.17.00216

Karidas, P., Challa, K. R., & Nath, U. (2015). The tarani mutation alters surface curvature in Arabidopsis leaves by perturbing the patterns of surface expansion and cell division. *Journal of Experimental Botany*, *66*(7), 2107–2122. https://doi.org/10.1093/jxb/erv015

Kim, D. I., & Roux, K. J. (2016). Filling the Void: Proximity-Based Labeling of Proteins in Living Cells. *Trends in Cell Biology*, *26*(11), 804–817. https://doi.org/10.1016/J.TCB.2016.09.004

Kurihara, D., Matsunaga, S., Omura, T., Higashiyama, T., & Fukui, K. (2011). *Identification and characterization of plant Haspin kinase as a histone H3 threonine kinase*. http://psort.nibb.ac.jp/form.html

Li, L., Nelson, C. J., Trösch, J., Castleden, I., Huang, S., & Millar, A. H. (2017). Protein degradation rate in Arabidopsis thaliana leaf growth and development. *Plant Cell*, *29*(2), 207–228. https://doi.org/10.1105/tpc.16.00768

Mair, A., Xu, S. L., Branon, T. C., Ting, A. Y., & Bergmann, D. C. (2019). Proximity labeling of protein complexes and cell type specific organellar proteomes in Arabidopsis enabled by TurboID. *ELife*, *8*, 1–29. https://doi.org/10.7554/eLife.47864

Majumdar, P., Karidas, P., Siddiqi, I., & Nath, U. (2020a). The ubiquitin-specific protease TNI/UBP14 functions in ubiquitin recycling and affects auxin response. *Plant Physiology*, *184*(3), 1499–1513. https://doi.org/10.1104/pp.20.00689

Majumdar, P., & Nath, U. (2020). De-ubiquitinases on the move: an emerging field in plant biology. *Plant Biology*, *22*(4), 563–572. https://doi.org/10.1111/plb.13118

Ramos, J. A., Zenser, N., Leyser, O., Callis, J., Ramos, J. A., Zenser, N., Leyser, O., & Callisa, J. (2022). *Rapid Degradation of Auxin / Indoleacetic Acid Proteins Requires Conserved Amino Acids of Domain II and Is Proteasome Dependent Linked references are available on JSTOR for this article : Rapid Degradation of Auxin / Indoleacetic Acid Proteins Requires Co*. *13*(10), 2349–2360.

Riechmann, J. L., Heard, J., Martin, G., Reuber, L., Jiang, C. Z., Keddie, J., Adam, L., Pineda, O., Ratcliffe, O. J., Samaha, R. R., Creelman, R., Pilgrim, M., Broun, P., Zhang, J. Z., Ghandehari, D., Sherman, B. K., & Yu, G. L. (2000). Arabidopsis transcription factors: Genome-wide comparative analysis among eukaryotes. *Science*, *290*(5499), 2105–2110. https://doi.org/10.1126/science.290.5499.2105

Roux, K. J., Kim, D. I., Raida, M., & Burke, B. (2012). A promiscuous biotin ligase fusion protein identifies proximal and interacting proteins in mammalian cells. *Journal of Cell Biology*, *196*(6), 801–810. https://doi.org/10.1083/jcb.201112098

Tzafrir, I., McElver, J. A., Liu, C. M., Li, J. Y., Wu, J. Q., Martinez, A., Patton, D. A., & Meinke, D. W. (2002a). Diversity of TITAN functions in Arabidopsis seed development. *Plant Physiology*, *128*(1), 38–51. https://doi.org/10.1104/pp.010911

Wang, Z., Zhang, H., Liu, C., Xing, J., & Chen, X. L. (2018). A deubiquitinating enzyme Ubp14 is required for development, stress response, nutrient utilization, and pathogenesis of Magnaporthe oryzae. *Frontiers in Microbiology*, *9*(APR), 1–14. https://doi.org/10.3389/fmicb.2018.00769

Xu, Y., Jin, W., li, N., Zhang, W., Liu, C., Li, C., & Li, Y. (2016). UBIQUITIN-SPECIFIC PROTEASE 14 interacts with ULTRAVIOLET-B INSENSITIVE 4 to regulate endoreduplication and cell and organ growth in Arabidopsis. *The Plant Cell*, *28*(May), tpc.00007.2016. https://doi.org/10.1105/tpc.16.00007

Zhou, H., Zhao, J., Cai, J., & Patil, S. B. (2017). UBIQUITIN-SPECIFIC PROTEASES function in plant development and stress responses. *Plant Molecular Biology*, *94*(6), 565–576. https://doi.org/10.1007/s11103-017-0633-5

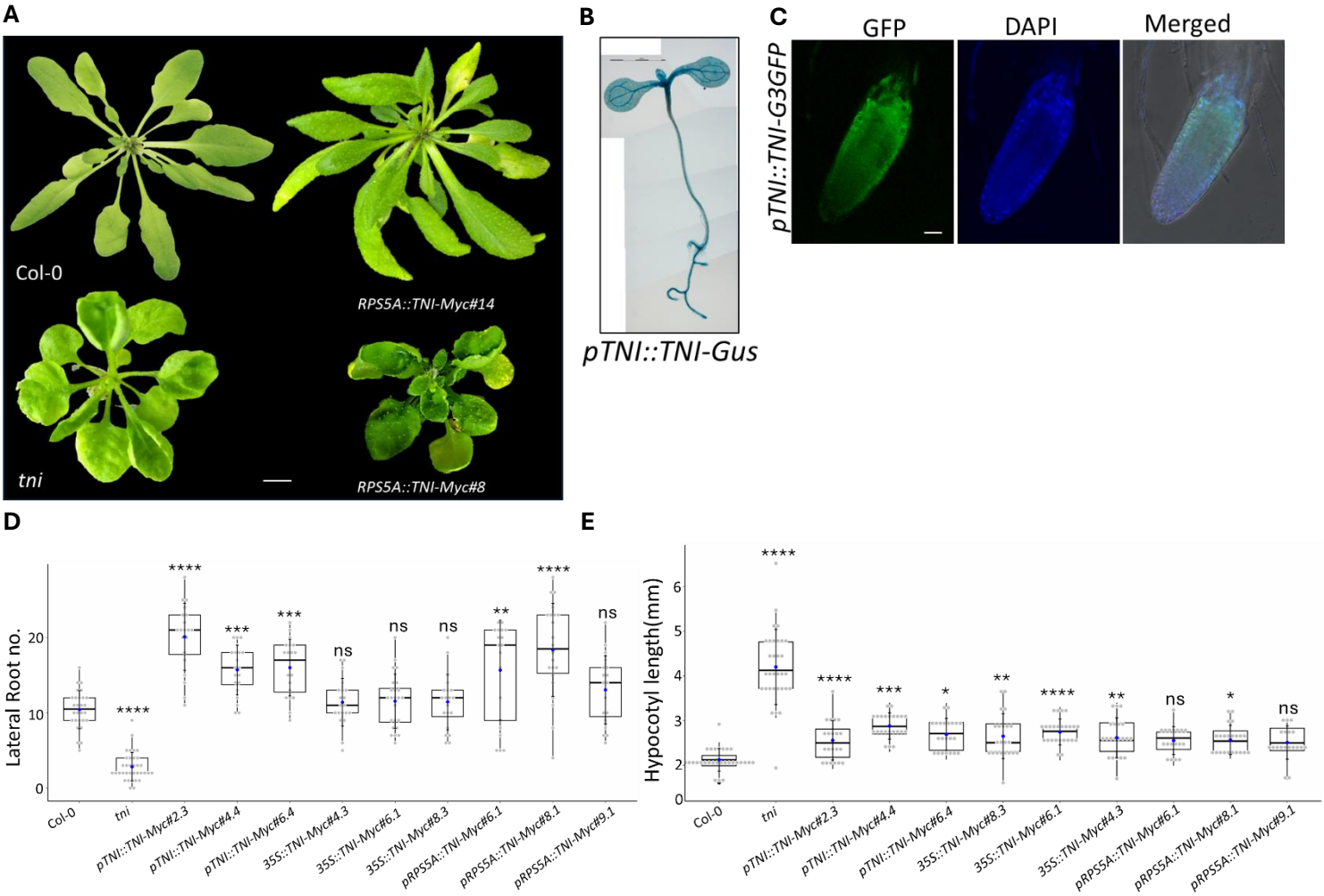

Figure 1. Phenotypic evaluation of *TNI* transgenic lines. (A) Top view of 30-day old rosettes of the indicated genotypes. Two independent transgenic plants overexpressing TNI-Myc fusion protein (*RPS5A::TNI-Myc#8 & RPS5A::TNI-Myc#14* are shown. Scale bar, 1 cm. (B) An 8-day old *pTNI::TNI-GUS* seedling processed for GUS activity. (C) Root tips of 8-day old *pTNI::TNI-G3GFP* seedlings showing TNI-GFP signal. DAPI staining visualises nuclei. (D-E) Average number (n = 25-30) of lateral roots (D) and average length of hypocotyl (E) in 12-day old (D) and 8-day old seedlings, respectively in the indicated genotypes. (). Error bars represent SD. Asterisks indicate significance using Tukey's *t*-test (**** $p<0.0001$, ***$p<0.001$, **$p<0.01$, *$p<0.1$, ns, not significant). Data are shown for nine independent transgenic lines.

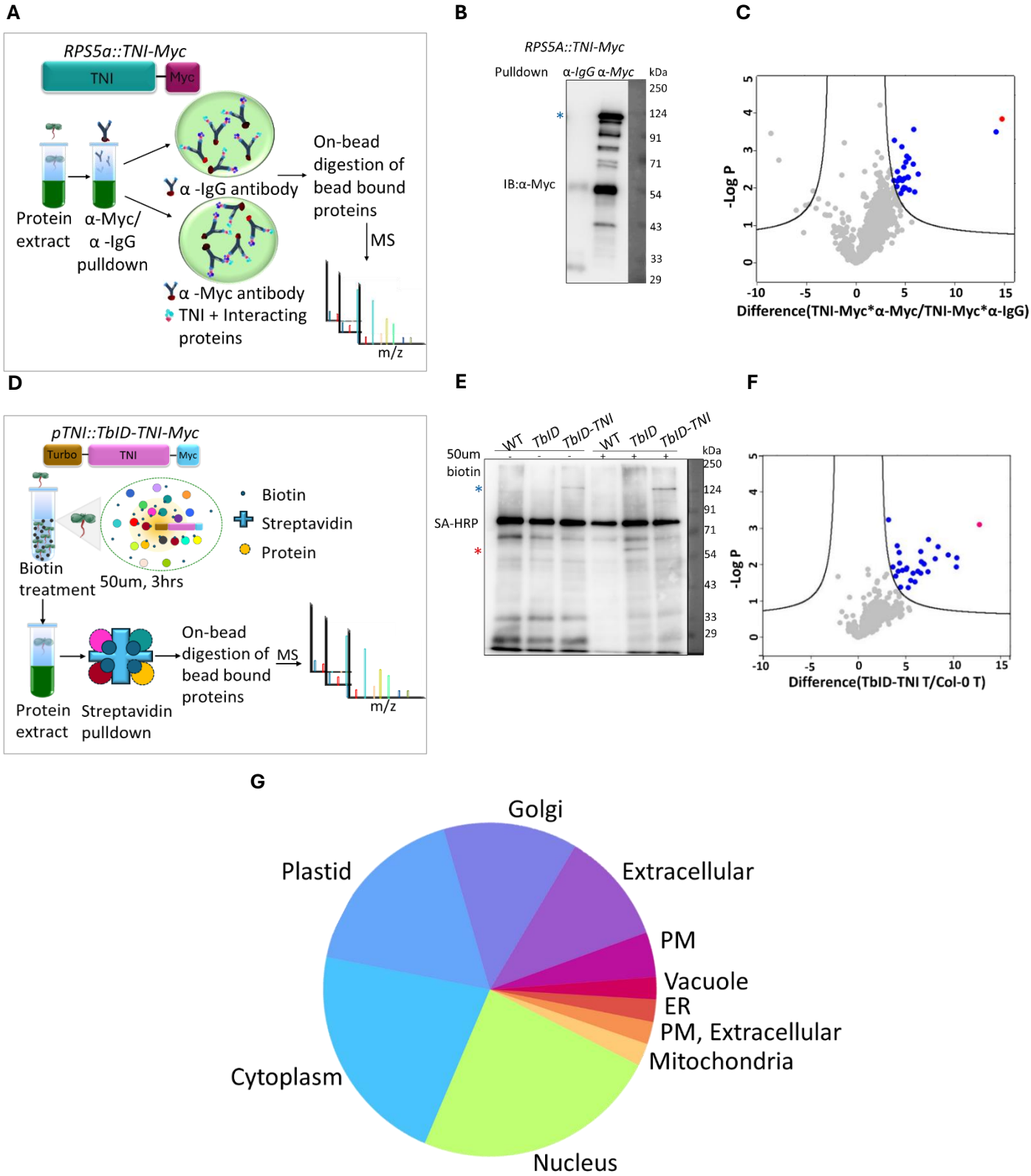

Figure 2. Identification of **TNI-interacting proteins by immunoprecipitation mass spectrometry (IP-MS) and affinity purification (AP-MS).** (A) A schematic description of the IP-MS experimental setup. Immuno-pulldown was performed by incubating total protein extract from *RPS5A::TNI-Myc* tissue with α-Myc and α-IgG (negative control) antibodies, followed by MS analysis. (B) A representative western blot image of TNI-Myc bait protein after pulldown with α-IgG or α-Myc antibodies. Experiment was repeated three times and similar results obtained. Blue asterisk corresponds to the TNI-Myc band. Numbers on the right indicate molecular-weight.

(C) Volcano plot showing proteins enriched in α-Myc pulldown sample over the α-IgG control in the IP-MS experiment described in (A-B). Blue circles, enriched proteins; red circle, TNI-Myc protein. (D) A schematic representation of the AP-MS experimental setup. Total protein extracts from 8-day old seedlings expressing *pTNI::TbID-TNI-Myc* and *pTNI::TbID-Myc* (negative control, not shown here) were treated with biotin, pulled-down by pulldown using streptavidin beads, followed by MS analysis (see *Methods* for more detail). (E) A representative western blot image of SA-HRP blot of streptavidin pulldown proteins from biotin untreated (-) and treated (+) Col-0, *pTNI::TbID-Myc,* and *pTNI::TbID-TNI-Myc* seedlings respectively. Experiment was repeated two times and similar results obtained. Blue and red asterisk corresponds to TNI-*TbID* and *TbID* bands respectively. Numbers on the right indicate molecular-weight. F) Volcano plot shows enriched proteins in biotin treated *TbID*-TNI (TbID-TNI T) Vs biotin treated Col-0 (Col-0 T) pulldown. Blue circles; enriched proteins, red circle; *TbID*-TNI, (G)TNI interactors identified through IP-MS and AP-MS are classified according to their subcellular localization. PM-Plasma Membrane; ER-Endoplasmic Reticulum.

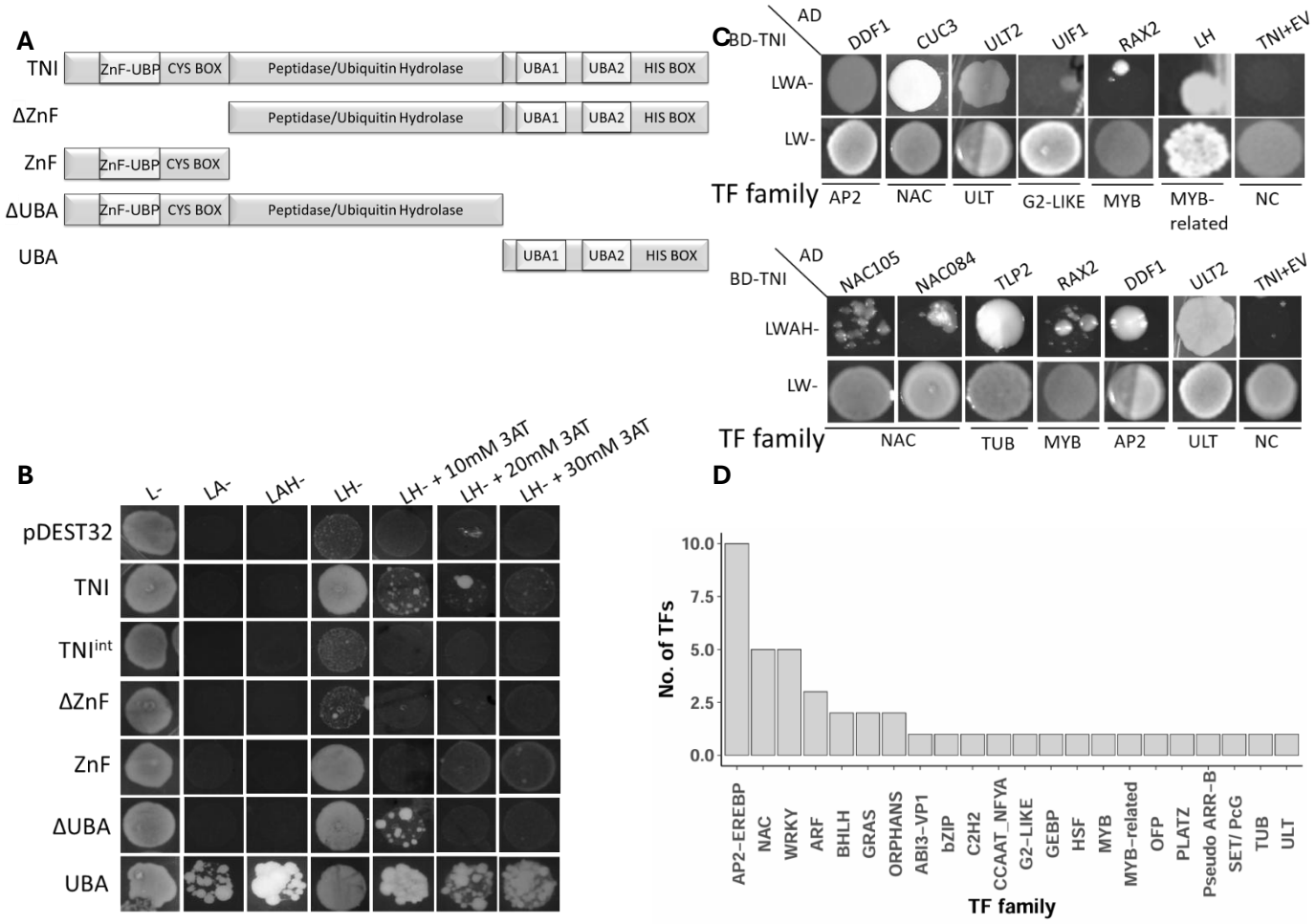

Figure 3. Yeast two-hybrid screen to identify TNI-interacting transcription factor (TF) proteins. (A) Schematics of full length TNI protein and its truncated forms (ΔZnF, ZnF, ΔUBA, UBA) used as baits in yeast two-hybrid screen. ZnF-UBP, Zinc finger-ubiquitin protease domain; UBA, ubiquitin-associated domain; CYS-BOX, cysteine box domain; HIS-BOX, histidine-box domain. (B) Autoactivation assay is performed for full-length TNI and its truncated forms mentioned in A. L, A & H indicate leucine, adenine & histidine, respectively; - indicates negative, AT indicates 3-amino-1,2,4-triazole (C) Representative images of yeast growth assay on selection plates after co-transformation with bait and prey constructs. Growth on LWA- plates signify interaction. Complete list of TFs showing interaction is shown in Table 1. BD, binding domain; AD, activation domain. (D) TFs identified in (C) as TNI-interacting proteins are categorized in different functional families.

Table 1. A comprehensive list of **TNI-interacting proteins.** TNI-interacting proteins identified in IP-MS (1-29), AP-MS (30-50), and yeast two-hybrid screen (51-95) are listed. Information on subcellular localization are from *SUBA5* database. AGI, Arabidopsis gene identifier in *TAIR* database; PM, plasma membrane, ER, endoplasmic reticulum.

Sl.No.	AGI	Protein	Gene name	Subcellular localization
1	AT1G09450	Haspin kinase	HASPIN	Nucleus
2	AT1G12900	Glyceraldehyde 3-phosphate dehydrogenase A subunit 2	GAPA-2	Plastid
3	AT1G43190	Polypyrimidine tract-binding protein 3	PTB3	Nucleus
4	AT1G79850	Ribosomal protein S17	RPS17	Plastid
5	AT2G01140	Fructose-Bisphosphate Aldolase 3	FBA3	Plastid
6	AT2G19830	SNF7 family protein	VPS32.1	Golgi
7	AT2G41100	Calmodulin-like 12, Touch3	CML12	Vacuole
8	AT3G11730	RAB GTPase homolog D1	RABD1	Golgi
9	AT3G13750	Beta galactosidase 1	BGAL1	Extracellular
10	AT3G13772	Transmembrane nine 7	TMN7	Golgi
11	AT3G18820	RAB GTPase homolog G3F	RABG3F	Golgi
12	AT3G44990	Xyloglucan endo-transglycosylase-related 8	XTH31	PM, Extracellular
13	AT3G52750	Tubulin/FtsZ family protein	FTSZ2-2	Plastid
14	AT4G08850	MDIS1-interacting receptor like kinase2	MIK2	PM
15	AT4G12880	Early nodulin-like protein 19	ENODL19	Extracellular
16	AT4G27640	Importin-beta 4 (IMB4)	T29A15.130	Nucleus
17	AT4G30170	Peroxidase family protein	PER45	Extracellular
18	AT4G39520	Developmentally regulated g-protein	DRG3, DRG1-1	Cytosol
19	AT5G06690	WCRKC thioredoxin 1	WCRKC1	Plastid
20	AT5G22040	Ubiquitin carboxyl-terminal hydrolase	Q9C584	Nucleus
21	AT5G26930	GATA transcription factor 23	GATA23	Nucleus
22	AT5G37780	Calmodulin 1	CAM1	Nucleus
23	AT5G47520	RAB GTPase homolog A5A	RABA5A	PM
24	AT5G49360	Beta-xylosidase 1	BXL1	Extracellular
25	AT5G51720	NEET group protein	NEET	Plastid
26	AT5G56870	Beta-galactosidase 4	BGAL4	Extracellular
27	AT5G60640	PDI-like 1-4	PDIL1-4	ER
28	ATCG00710	Photosystem II reaction center protein H	PSBH	Plastid
29	ATCG01300	Ribosomal protein L23	RPL23-A	Plastid
35	AT3G01540	DEAD box RNA helicase 1	DRH1, RH14	Nucleus
36	AT3G11400	Elongation Initiation Factor 3	EIF3G1	Cytosol
37	AT3G15730	Phospholipase D alpha 1	PLDALPHA1	Cytosol
38	AT3G51800	ERBB-3 Binding Protein 1	EBP1, ATG2	Cytosol
39	AT3G59770	Suppressor of Actin 9	SAC9	Golgi
40	AT3G60190	Dynamin-like 1E	DRP1E	Cytosol
41	AT3G61220	Short-chain Dehydrogenase	SDR1	Cytosol
42	AT4G02450	HSP20-like chaperones superfamily protein	P23-1	Nucleus
43	AT4G02510	Translocon at outer envelope membrane of chloroplasts 159	TOC159	Plastid
44	AT4G24800	EIN2 C-Terminus Interacting Protein 1	ECIP1, MRF3	Golgi
45	AT5G13490	ADP/ATP carrier 2	AAC2	Mitochondria
46	AT5G15970	Stress-responsive protein	KIN2, COR6	Cytosol
47	AT5G16840	Binding partner of acd11 1	BPA1	Nucleus
48	ATCG01110	NAD(P)H dehydrogenase subunit H	NDHH	Plastid

49	AT1G01060	Late Elongated Hypocotyl 1	LHY 1	Nucleus
50	AT1G04050	Homolog of SU(var)3-9 1	SUVR1	Nucleus
51	AT1G12610	Dwarf and Delayed Flowering 1	DDF1	Nucleus
52	AT1G13600	Basic Leucine-Zipper 58	BZIP58	Nucleus
53	AT1G19050	Arabidopsis Response Regulator	ARR7	Nucleus
54	AT1G22490	Basic helix-loop-helix 94	BHLH94	Nucleus
55	AT1G22810	Ethylene Response Factor 19	ERF19	Nucleus
56	AT1G62300	WRKY family transcription factor 6	WRKY6	Nucleus
57	AT1G64380	Ethylene Response Factor 61	ERF61	Nucleus
58	AT1G66350	RGA-like 1	RGL1	Nucleus
59	AT1G76420	Cup Shaped Cotyledon 3	CUC3	Nucleus
60	AT1G79700	Wrinkled 4	WRI4	Nucleus
61	AT2G18060	Vascular related NAC-domain protein 1	VND1	Nucleus
62	AT2G18280	Tubby Like Protein 2	TLP2	Golgi
63	AT2G20825	Ultrapetala 2	ULT2	Nucleus
64	AT2G20880	Ethylene Response Factor 53	ERF53	Nucleus
65	AT2G32100	Ovate Family Protein 16	OFP16	Nucleus
66	AT2G36890	Regulatory of Axillary Meristem 2	RAX2	Nucleus
67	AT2G37430	C2H2 and C2HC zinc fingers superfamily protein	ZAT11	Nucleus
68	AT2G46790	Pseudo-Response Regulator 9	PRR9	Nucleus
69	AT3G01600	NAC domain containing protein 44	NAC044	Nucleus
70	AT3G05690	Nuclear Factor Y	NF-YA2	Nucleus
71	AT3G23220	Ethylene Response Factor 95	ERF95/ESE1	Nucleus
72	AT3G23230	Ethylene Response Factor 98	ERF98	Nucleus
73	AT3G23240	Ethylene Response Factor 1B	ERF1B	Nucleus
74	AT3G50330	HECATE 2	HEC2	Nucleus
75	AT3G51910	Heat Shock Transcription Factor A7A	HSF7A	Nucleus
76	AT3G61830	Auxin Response Factor 18	ARF18	Nucleus
77	AT4G00390	DNA-binding storekeeper protein-related transcriptional regulator	GeBP, F5I10.6	Nucleus
78	AT4G01500	NGATHA4	NGA4	Nucleus
79	AT4G17230	SCARECROW-like 13	SCL13	Nucleus
80	AT4G17900	PLATZ 11	T6K21.80	Nucleus
81	AT4G23980	Auxin Response Factor 9	ARF9	Nucleus
82	AT4G30080	Auxin Response Factor 1	ARF1	Nucleus
83	AT4G37180	Ultrapetala Interacting Factor 1	UIF1, HHO5	Nucleus
84	AT5G07100	WRKY DNA-binding protein 26	WRKY26	Nucleus
85	AT5G14000	NAC domain containing protein 84	NAC084	Nucleus
86	AT5G24110	WRKY DNA-binding protein 30	WRKY30	Nucleus
87	AT5G26170	WRKY DNA-binding protein 50	WRKY50	Nucleus
88	AT5G47230	Ethylene Responsive element binding Factor 5	ERF5	Nucleus
89	AT5G54470	B-Box type zinc finger family protein 29	BBX29	Nucleus
90	AT5G64750	ABA Repressor 1	ABR1	Nucleus
91	AT5G64810	WRKY DNA-binding protein 51	WRKY51	Nucleus
92	AT5G66300	NAC domain containing protein 105	NAC105	Nucleus

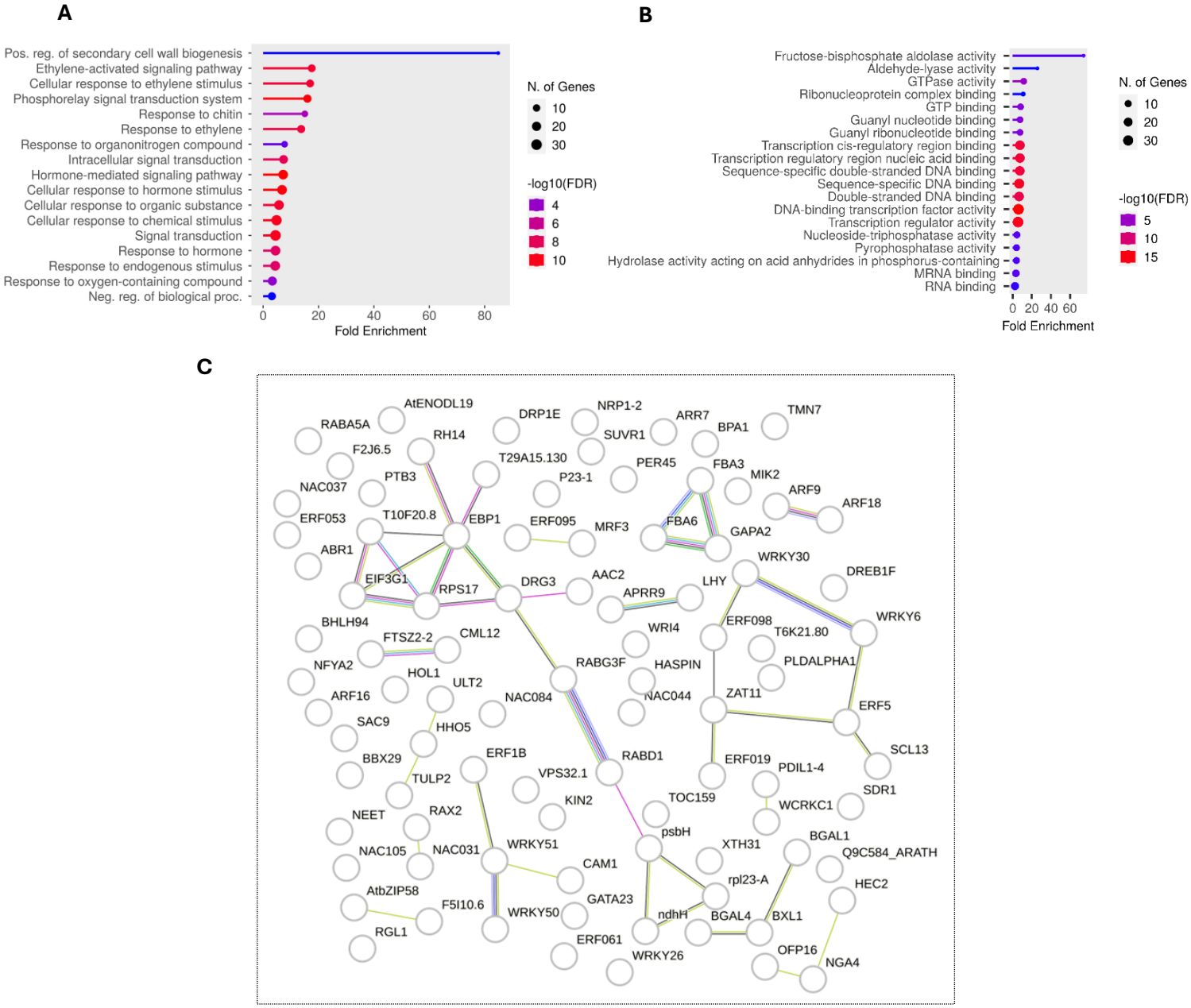

Figure 4. Gene ontology (GO) analysis of the TNI-interacting proteins. GO analysis performed according to biological processes (A) and molecular function (B). (C) An interaction network of all TNI-interacting proteins obtained from the STRING database. Colour of the edge depicts the method of protein identification (known interactions, pink; experimentally-determined interactions from curated databases, navy blue; predicted interactions, green; gene neighbourhood, red; gene fusion, blue; gene co-occurrence, light green; text mining, black; co-expression, light blue; protein homology.

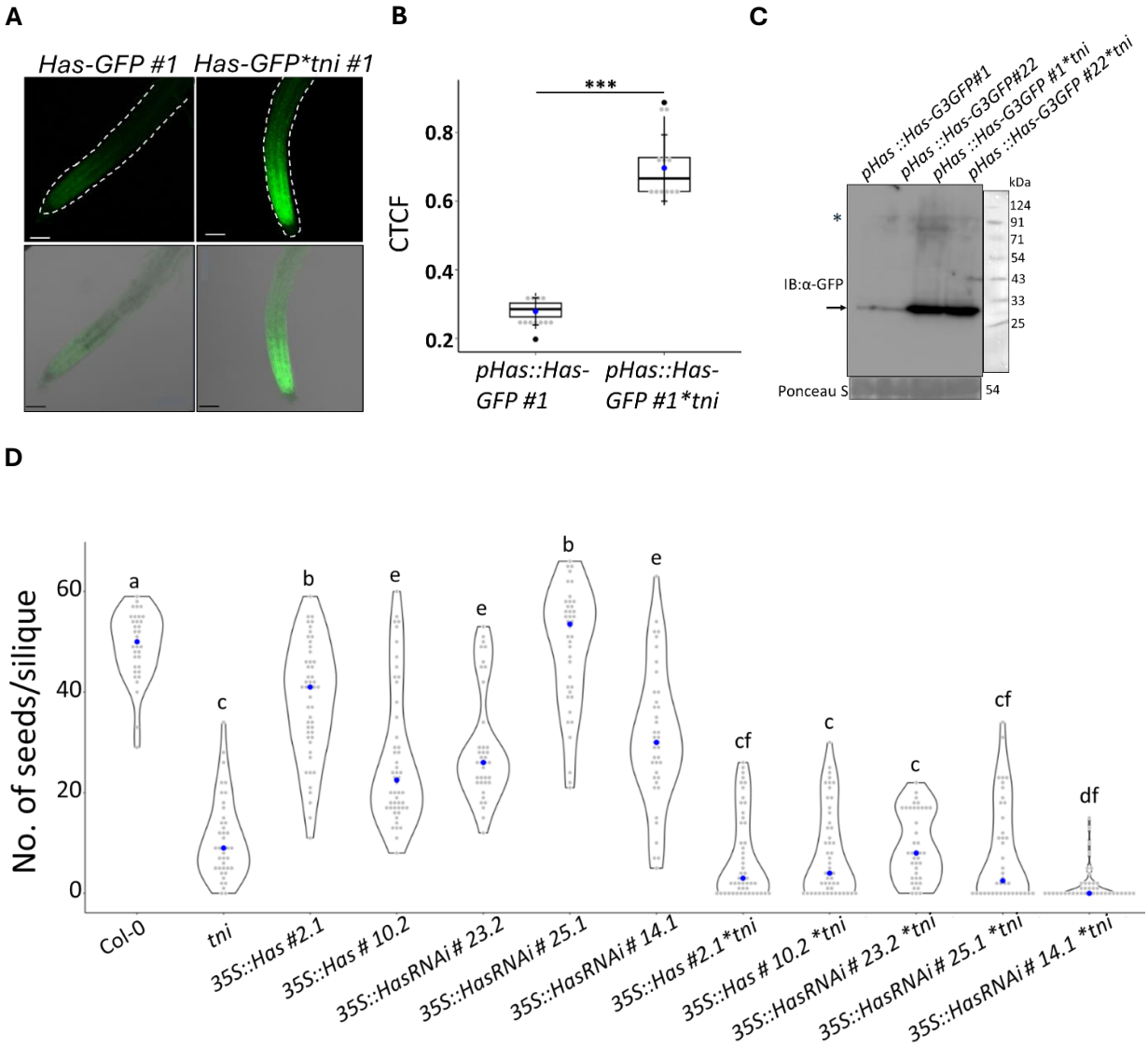

Figure 5. Haspin kinase is stabilised in the *tni* mutant. (A, B) Images of root tips (A) of 8-day old *pHAS::Haspin-GFP* and *pHAS::Haspin-GFP*tni* seedlings showing GFP fluorescence (#1 indicates line number), and average quantification (n=11) of fluorescent intensity (B). CTCF indicates Corrected Cell Fluorescence Intensity. Error bars represent the SD; asterisk indicates statistical significance using unpaired Student's *t* test (*** $p = 0$). Scale bar in (A), 100 µm. (C) Image of western blot of total protein extracted from 8-day old seedlings of indicated genotypes and probed with α-GFP antibody. Asterisk and arrow correspond to Has-GFP protein band and cleaved GFP protein, respectively. Ponceau staining shown below the western blot served as the loading control. Numbers on the right indicate molecular weight. (D) Average number of seeds per silique (n = 35-40) in the indicated genotypes. Numbers on the right indicate independent transgenic events. Each grey dot indicates number of seeds in a silique. Blue circle represents the median. Groups indicated by the same letter are not statistically different according to ANOVA with Tukey's HSD test.

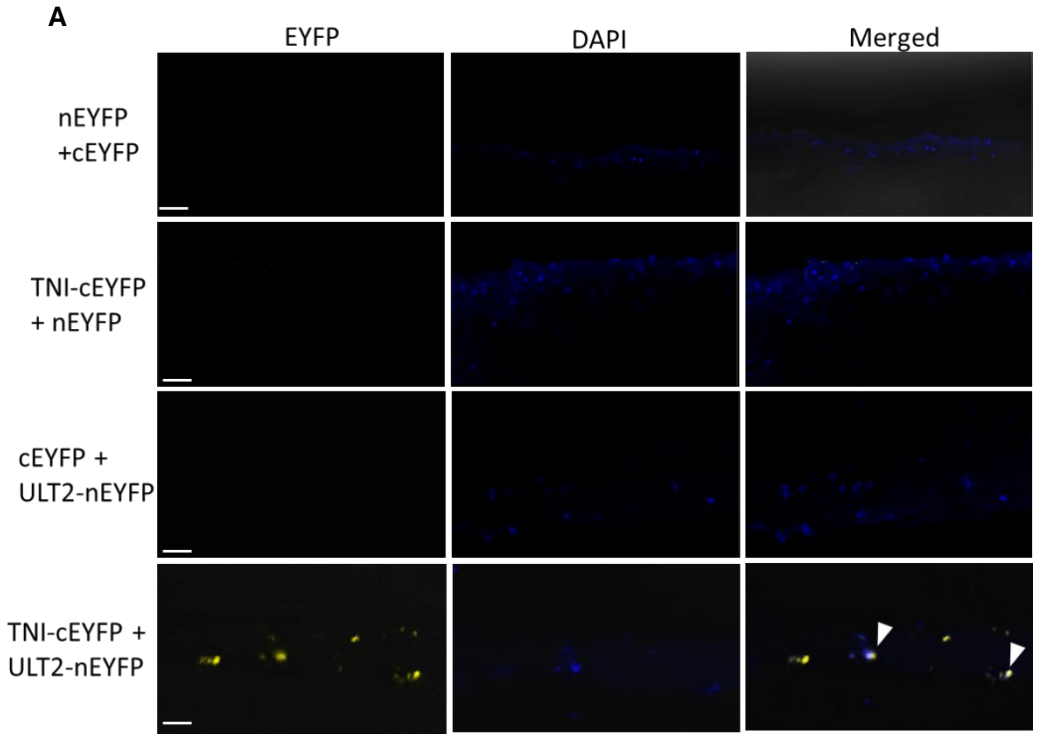

Figure 6. In vivo interaction of TNI with ULT2. Bimolecular fluorescence complementation assay of TNI-cEYFP and ULT2-nEYFP transiently expressed in tobacco leaves. Images of the abaxial epidermal cells were taken 48-72 hrs post-infiltration. EYFP fluorescence, DAPI fluorescence, and merged images are shown. Images in the first three rows serve as negative controls. The fourth lane shows co-infiltrated test proteins TNI-cEYFP and ULT2-nEYFP proteins interacting in the nucleus (white arrowhead). Scale bar, 50 µm.